DOI: 10.61782/fa.2025.0584

FORUM ACUSTICUM EURONOISE 2025

MOMENTUM ALGORITHM AND ITS APPLICATION TO ACTIVE CONTROL OF HVAC COMPRESSOR NOISE IN AUTONOMOUS BUS

Sang-Kwon Lee[1*] **Junseok Choi**[1]
Doyeon Kim[1] **Seongyeol Kim**[1]
[1] Department of Mechanical Engineering, Inha University, South Korea

ABSTRACT

The compressor is used for a heating, ventilation, and air-conditioning (HVAC) system which provide air conditioning for each passenger in autonomous bus. The sound radiated from the compressor of the HVAC system is a high-frequency annoyance noise caused by vibroacoustic noise due to the shell vibration of the compressor. The dominant frequency components of the vibroacoustic noise are harmonics of the rotation frequency of the reciprocating compressor. The HVAC system generates vibroacoustic noise dominantly in the frequen-cy range between 100 and 600 Hz. Such noise is not only distinctly perceptible but also contributes to passenger discomfort and negatively impacts the perceived quality of the vehicle. The aim of this paper is to attenuate the vibroacoustic noise of the HVAC system by developing an active noise control (ANC) system. Generally, the widely recognized filtered-X least mean squared (FXLMS) algorithm has been successfully implemented to active noise control of reciprocating compressor. However, its performance was found lacking outside the peak frequency of compressor operation noise. To address this, the momentum algorithm was employed to enhance ANC performance. The momentum algorithm has a lower residual error and faster convergence rate compared to the FXLMS algorithm. As a consequence, the implementation of the momentum based ANC algorithm resulted in enhanced noise reduction not only at the peak frequencies, which correspond to the compressor operation frequency, but also in frequency ranges outside these peak frequencies.

[*]***Corresponding author***: *sangkwon@inha.ac.kr*

Keywords: *compressor, vibroacoustic noise,active noise control, momentum algorithm, fast convergence.*

1. INTRODUCTION

HVAC noise profoundly affects passenger riding comfort within electric vehicle cabins. Consequently, extensive re-search efforts have been devoted to analyzing and reduc-ing these noises. Contrasting with typical vehicle HVAC systems, the HVAC system under autonomous bus seats is structurally akin to refrigerator systems, incorporating com-ponents like compressors, evaporators, condensers, and fans. This similarity allows for the application of noise con-trol techniques used in refrigerator systems to be effectively employed in autonomous car seat HVAC systems as shown in Fig.1. Among these HVAC parts, the shell vibration of the compressor generates noise that is harmonic to the rotation frequency of the reciprocating compressor. The hybrid technique, a combination of passive and active techniques, can be used to obtain a reduction in the overall frequency range for this dominant noise.

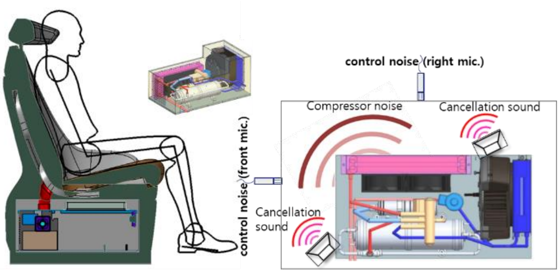

Figure 1. HVAC system of autonomous bus seat.

ANC stands out as a technique for suppressing low-frequency noise, offering the advantage of effective noise reduction without additional weight or space consumption unlike many passive methods [1]. On the other hand, passive strategies such as sound absorbing materials are more suited for high-frequency noise reduction [2]. For example, the vibration absorber can be designed to reduce such structural vibration in the high-frequency range [3]. ANC operates by producing ’anti-noise’ of equal amplitude but opposite phase to the primary noise. Adaptive filter-ing, often employing the LMS algorithm, is a cornerstone of ANC systems for addressing time-varying noise characteris-tics [4]. Despite its effectiveness, there are space con-straints within the system that limit the speaker size, affecting low-frequency noise reduction. Therefore, the low-frequency component of the output can be filtered out [5]. In this study, on the other hand, a frequency range between 200 Hz and 600 Hz is targeted for this ANC application since the speaker to be used has a diameter of 2.25 inches. However, this frequency range is relatively high for the ANC ap-plication because the generation of a signal that is out of phase of the high-frequency primary noise signal is chal-lenging due to its short wavelength. Hence, the ANC algo-rithm requires fast convergence. For the ANC algorithm, the FXLMS algorithm is widely used because it is robust and requires low computation. However, the convergence speed of the LMS algorithm is poor due to a phenomenon called eigenvalue spread [6]. The performance of the LMS algo-rithm can be improved using the momentum algorithm [7] with a small increase in computational burden In this study, the momentum algorithm based ANC algorithm will be de-veloped for the HVAC system for autonomous bus seats.

2. FXLMS ALGORITHM

The fundamental objective of the Least Mean Square (LMS) algorithm is to compute the optimal filter coefficients that minimize the mean square error. This optimization employs the iterative steepest descent method, where each iteration proceeds in the direction opposite to the gradient of the error surface [4].

$$\boldsymbol{w}(n+1) = \boldsymbol{w}(n) + \mu(-\nabla_n) \tag{1}$$

The error signal, $e(n)$, is defined as the difference between the desired signal (in this case, noise to be canceled), $d(n)$, and the output signal, $y(n) = x(n)\boldsymbol{w}(n)$.

$$e(n) = d(n) - x(n)\boldsymbol{w}(n) \tag{2}$$

Accordingly, the gradient of the squared error is expressed as

$$\nabla e^2(n) = -2e(n)x(n) \tag{3}$$

Substituting Eq. (3) into Eq. (1), the final form of the LMS algorithm is obtained.

$$\boldsymbol{w}(n+1) = \boldsymbol{w}(n) + \mu x(n)e(n) \tag{4}$$

Here, μ denotes the convergence factor, crucial for the stability and steady-state performance of the algorithm. The algorithm employs a time-varying step size, calculated to be inversely proportional to both the power of the reference signal ($\widehat{P_x}$) and the filter length (L). This is expressed as

$$\mu(n) = \frac{\alpha}{L\widehat{P_x}(n)} \tag{5}$$

Here, the normalized step size α falls within the range of $0 < \alpha < 2$. The power of the reference signal is estimated using the formula.

$$\widehat{P_x}(n) = \frac{1}{M}\sum_{m=0}^{M-1} x^2(n-m) \tag{6}$$

To mitigate divergence issues due to insufficient spectral excitation, a leaky mechanism is integrated into the weight update process. The leaky LMS algorithm is thus formulated as follows.

$$\boldsymbol{w}(n+1) = \nu\boldsymbol{w}(n) + \mu x(n)e(n) \tag{7}$$

In this context, ν denotes the leakage factor, constrained within the range $0 < \nu \leq 1$. Adjusting the leakage factor involves a trade-off between robustness and performance loss [1]. In practical implementations involving electronic components such as microphones, filters, and amplifiers, the signal path from the loudspeaker to the error microphone, termed the secondary path, significantly influences the ANC system’s efficacy. Burgess [8] proposed compensating for the secondary path effect to enhance system performance. This is achieved by filtering the reference signal with a filter that mimics the secondary path, leading to the development of the filtered-X LMS (FXLMS) algorithm. The error signal in the FXLMS context is redefined as follows.

$$\hat{x}(n) = s(n) * x(n) \tag{8}$$

where $s(n)$ is the impulse response of the secondary path, $*$ denotes linear convolution. The gradient of squared error can be rewritten as

$$\nabla e(n) = -2\hat{x}(n)e(n). \tag{9}$$

The FXLMS algorithm iteratively updates the filter weights to achieve optimum noise cancellation.

$$\boldsymbol{w}(n+1) = \nu\boldsymbol{w}(n) + \mu\hat{x}(n)e(n) \tag{10}$$

Since the transfer function, $S(z)$ of the secondary path is typically unknown, it can be estimated via a separate LMS algorithm. The adaptive filter output is computed by linear convolution between the optimum filter and the reference signal.

$$y(n) = \sum_{l=0}^{L} w_l(n)\hat{x}(n-l) \tag{11}$$

The block diagram of the FXLMS algorithm is shown in Fig. 2.

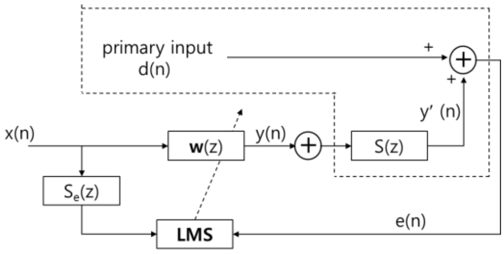

Figure 2. Block diagram of ANC system using FXLMS algorithm.

In this representation, $\hat{S}(z)$ denotes the estimated transfer function of the secondary path, $P(z)$ represents the primary path, and $W(z)$ symbolizes the time-varying adaptive filter.

3. THEORY OF THE MOMENTUM ALGORITHM

The momentum algorithm can also be derived from gradient descent method, where the gradient of gradient descent descends along the surface of cost function ξ which is error surface in the context of ANC. The system can resemble to dynamic system with a mass moving along the error surface. The direction of movement at this time is determined by potential $\nabla\xi$, and can be expressed as [9]

$$\frac{d\boldsymbol{w}}{dt} = \nabla\xi \tag{12}$$

Therefore, in (12), while a local minimum is achieved when $\nabla\xi(\boldsymbol{w}) = 0$, it is not the only equation where a minimum point occurs exactly at $\nabla\xi(\boldsymbol{w}) = 0$ but also governs the system movement. In other words, the system does not converge directly to the target point but rather oscillates and gradually converges. This can be considered as a simple oscillator that takes into account the oscillations that occur. Using this, the resulting second-order differential equation is as

$$\eta\frac{d^2\boldsymbol{w}}{dt^2} = -\nabla\xi(\boldsymbol{w}) - b\frac{d\boldsymbol{w}}{dt} \tag{13}$$

If $\eta \geq 0$, it considers the mass of the particle, and if $b \geq 0$, t considers the damping that occurs during the system's change process. When $\nabla\xi(\boldsymbol{w}) = 0$ as in (12), it reaches a minimum point in the differential equation. When η converges to 0, it results in (12). If η is positive, the trajectory represented by (13) gradually changes direction in the direction indicated by $-\nabla\xi(\boldsymbol{w})$, showing evidence of momentum [9]. A simple finite difference approximation in (13) is as

$$\eta\frac{\boldsymbol{w}(t+\Delta t) - 2\boldsymbol{w}(t) + \boldsymbol{w}(t-\Delta t)}{(\Delta t)^2} \approx -\nabla\xi(\boldsymbol{w}(t)) - b\frac{\boldsymbol{w}(t+\Delta t) - \boldsymbol{w}(t)}{\Delta t} \tag{14}$$

In summary,

$$\boldsymbol{w}(t+\Delta t) = \boldsymbol{w}(t) - \alpha\nabla\xi\big(\boldsymbol{w}(t)\big) + \beta(\boldsymbol{w}(t) - \boldsymbol{w}(t-\Delta t)) \tag{15}$$

In the ANC system, signals are processed as discrete signals rather than continuous signals, so $t = n$, $\Delta t = 1$. Therefore, equation (15) can be rearranged for discrete signals as

$$\boldsymbol{w}(n+1) = \boldsymbol{w}(n) - \alpha\nabla\xi\big(\boldsymbol{w}(n)\big) + \beta\big(\boldsymbol{w}(n) - \boldsymbol{w}(n-1)\big) \tag{16}$$

This algorithm is defined as Polyak's heavy ball method. With slight modifications, a related method called Nesterov's optimization can also be obtained. If ξ is a convex quadratic equation, the approach in (16) (allowing for adaptive choices of α and β that vary with each iteration) is called the Chebyshev iteration method. Additionally, (16) can be redefined as

$$\begin{aligned} \boldsymbol{v}(n) &= \boldsymbol{w}(n+1) - \boldsymbol{w}(n) \\ &= -\alpha\nabla\xi\big(\boldsymbol{w}(n)\big) + \beta\big(\boldsymbol{w}(n) - \boldsymbol{w}(n-1)\big) \\ &= -\alpha\nabla\xi\big(\boldsymbol{w}(n)\big) + \beta\boldsymbol{v}(n-1) \end{aligned} \tag{17}$$

In (17), we can divide it into two equations as follows.

$$\begin{cases} \boldsymbol{w}(n+1) = \boldsymbol{w}(n) + \boldsymbol{v}(n) \\ \boldsymbol{v}(n) = -\alpha\nabla\xi\big(\boldsymbol{w}(n)\big) + \beta\boldsymbol{v}(n-1) \end{cases} \quad (18)$$

Here, $\boldsymbol{v}$ is the accumulated gradient, $\boldsymbol{\alpha}$ is the step size, and β represents inertia, where $0 < \beta < 1$ and typically $\beta = 0.9$ is used. Additionally, $\nabla\xi(\boldsymbol{w}(n))$can be expressed as $\nabla\xi(n)$ in (12), and $\nabla\xi(\boldsymbol{w}(n))$ in (18) can be expressed by (9) as

$$\nabla\xi(\boldsymbol{w}(n)) = 2[\nabla \mathrm{e}(n)]\mathrm{e}(n) = -2\boldsymbol{x}(n)e(n) \quad (19)$$

By (19), (18) can be expressed as

$$\begin{cases} \boldsymbol{w}(n+1) = \boldsymbol{w}(n) + \boldsymbol{v}(n) \\ \boldsymbol{v}(n) = \mu\boldsymbol{x}(n)e(n) + \beta\boldsymbol{v}(n-1) \end{cases} \quad (20)$$

μ represents the step size. In other words, μ is a convergence coefficient that is crucial for stability and steady-state performance, much like in the LMS algorithm.

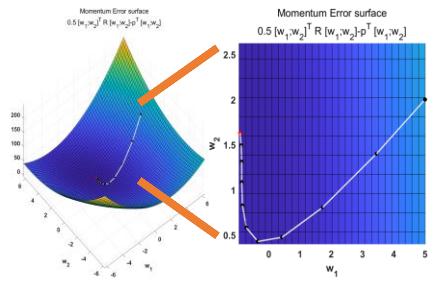

(a) Convergence of the momentum algorithm along the error surface.

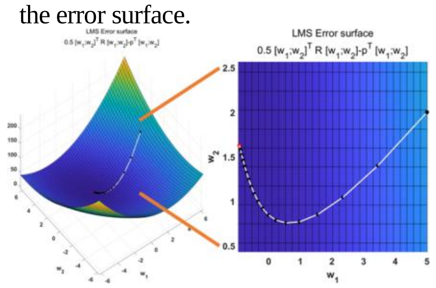

(b) Convergence of the LMS algorithm along the error surface.

Figure 3. Comparison of convergence performance the momentum and LMS algorithm along the error surface.

Therefore, the convergence performance depends on this μ value, and an appropriate μ value must be found. For an arbitutary cost function, the convergence pergormance of two algorithms along the error surface was comparied and its results are illustrated in Fig. 3.

4. ANC OF HVAC COMPRESSOR NOISE

4.1 Flow Chart of Algorithm

The ANC system employed in this study is characterized as a single reference with a multiple output configuration (1x2x2), as delineated in Fig. 4. The system acquires a reference signal through an accelerometer stuck to the compressor's shell. Two small size speakers were useded for ANC. One speaker positioned at the front side of compressor and the other one is right side. The error signals were captured by microphones strategically placed in the near field of the front and right sides of the HVAC system. These reference and error signals are crucial in the computation of filter coefficients, a process executed utilizing Eq. (10) and Eq. (20). It should be noted that the reference signal undergoes a filtration process before its integration into the algorithm, facilitated by modeled secondary filters. These filters represent transfer functions that cover the characteristics of various electronic components, such as analog filters and amplifiers, as well as the acoustic pathway extending from the speakers to the error microphones. Subsequently, the derived optimal filter coefficients are convolved with the reference signal in accordance with Eq. (11). This process yields the output signal $y(n)$, which functions as the anti-noise of the targeted noise signal $d(n)$.

4.2 Experimental Setup of the HVAC ANC System

The experimental setup entailed the utilization of a notebook computer interfaced with the dSPACE Autobox I/O board as shown in Fig. 5. The dSPACE Autobox plays a crucial role in this setup, facilitating the conversion of signals from analog to digital and vice versa. Additionally, it executes the embedded MATLAB Simulink code designated for Active Noise Control (ANC).

The signals collected from the error microphones and the accelerometer cannot be employed in their raw form due to the indeterminate frequency content. Consequently, it becomes essential to subject these signals to a low-pass filtering process. This step aids in determining the appropriate sampling frequency. The low-pass filters are configured with a cut-off frequency of 400 Hz in this study, marginally exceeding the highest frequency target for ANC.

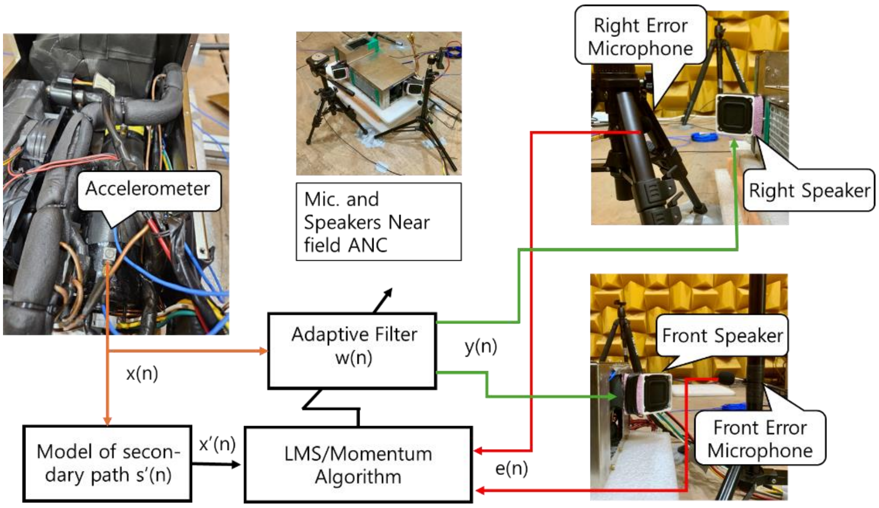

Figure 4. Block diagram of ANC system using FXLMS algorithm.

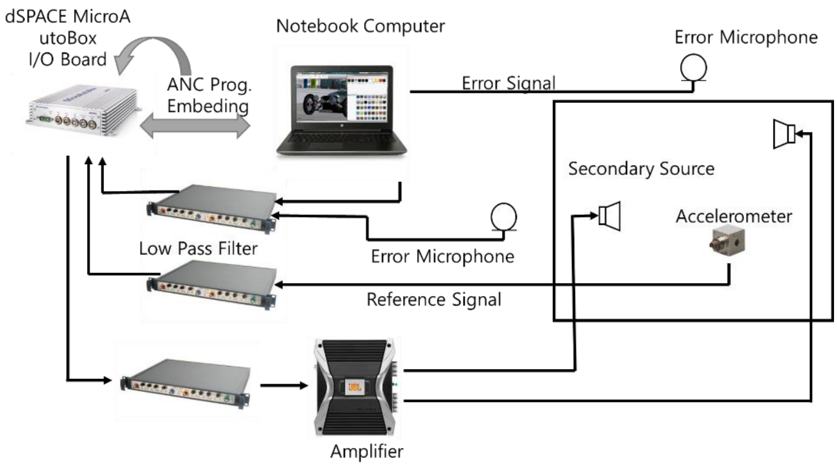

Figure 5. Experimental setup for the implementation of ANC system.

To prevent the occurrence of aliasing which distorts the signal, the sampling frequency must be at least twice the frequency content of the signal according to the Nyquist-Shannon sampling theorem. In this instance, a sampling frequency of 2048 Hz is selected, exceeding the double threshold of the signal's frequency content. Moreover, the output signal $y(n)$, directed towards the speakers, requires filtering to correct any reconstruction errors that may arise during the digital-to-analog (A/D) conversion process. Therefore, the cut-off frequency for this reconstruction filter is set at 400 Hz to eliminate the reconstruction error during the A/D conversion and to prevent the algorithm from diverging due to exciting the speakers outside the target frequency range (100-400 Hz). Finally, this signal is amplified using an amplifier to effectively drive the loudspeakers.

4.3 Placement of Error Microphones

To measure the basic SPL (sound pressure level) of HVAC system, five microphones have been installed within a 1-meter distance from the center of HVAC system in accordance with the stipulated standards [10] as shown in Fig. 6. According to the results of measured SPL, overall A-weighted SPL in frequency range (0-5000 Hz) was as listed in Tab. 1.

Table 1. A-weighted sound pressure level of all microphones.

Microphones	Front	Right	Left	Rear	Top
Average SPL	80.1 dB	83.2 dB	75.8 dB	77.1 dB	78.3 dB

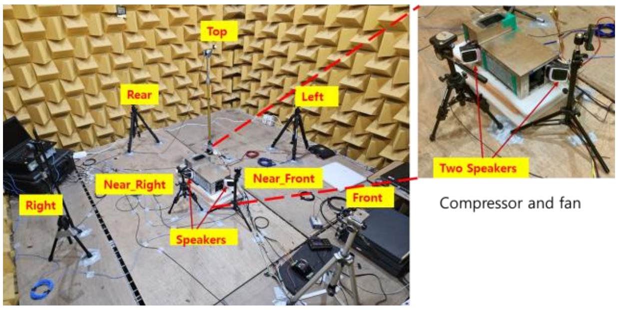

Figure 6. Setup of seven microhones and two speakers for ANC of HVAC system.

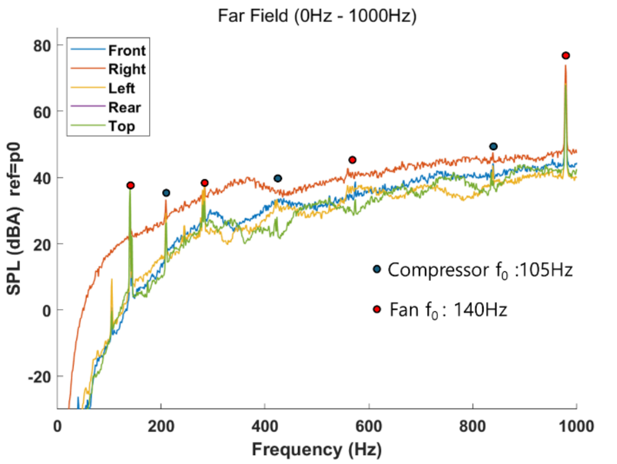

Figure 7. Frequency analysis of the sound pressure measured at the five microphones.

The major frequencies of the measured noise are associated to the rotating frequency of compressor shaft (105Hz) and cooling fan (140Hz) and their harmonics as shown in Fig.7. For the active cancellation of vibroacoustic noise radiated from shell of compressor and fan at nearfield, the error $e(n)$ microphones were installed at the front and the right of test compressor respectively. Two secondary speakers were also installed near to the test compressor as shown in Fig. 6. The frequency band that ANC is possible is from 100Hz to 400Hz due to size limit of secondary speaker and wave length of sound.

4.4 Selection of the Reference Signal

The ordinary coherence function is commonly employed to assess the extent of linear association between two signals, such as input and output signals [11]. The coherence value, therefore, is an important parameter for the performance evaluation of the ANC system [1]. Thus, magnitude-squared coherence can be defined as

$$C_{dx}(f) = |\gamma_{dx}(f)|^2 = \frac{|S_{dx}(f)|^2}{S_{dd}(f)S_{xx}(f)} \tag{21}$$

where f denotes the frequency of interest, $S_{dx}(f)$ is the cross-power spectrum, and $S_{dd}(f)$ and $S_{xx}(f)$ are the autopower spectra of $d(n)$ and $x(n)$, respectively. The coherence values between the accelerometer signal in the z direction and front, right microphone approached unity at the operational frequency of the compressor and its harmonics. This indicates a high degree of correlation, suggesting that the vibroacoustic noise emanating from the compressor can be effectively controlled.

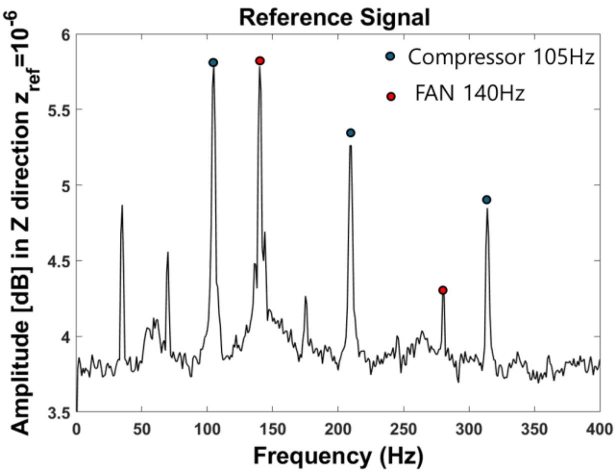

Figure 8. Fourier transform of the reference signal.

This indicates a high degree of correlation, suggesting that the vibroacoustic noise emanating from the compressor can be effectively controlled. According to the coherence results, the accelerometer data specifically collected in the z-axis direction has been employed as the reference signal $x(n)$ as shown in Fig. 4. The Fourier transform of this reference signal is presented in Fig.8, offering a detailed spectral representation. The peaks in the graph denote the operation frequency of the compressor and fan.\

4.5 Measurement of Secondary Paths

The estimation of the secondary path models, which are the transfer functions between speakers and error microphones, is based on the assumption that these models are time-invariant. Consequently, an offline modeling technique has been implemented to determine these filter coefficients. Broadband white noise, recognized as the ideal signal for such estimations due to its encompassing frequency range, is utilized in this process. This white noise is inputted into the speakers, and the consequent sound pressure is measured by the error microphones. Utilizing adaptive filter algorithms in this context facilitates the determination of the filter coefficients for the secondary paths, thereby allowing for a precise model estimation [12-13].

4.6 Results of the ANC

In this study, the momentum algorithm was used for the ANC of compressor and fan noise. The discrete Fourier transforms (DFTs) of the signals captured by the error microphones are graphically represented in Fig. 9. Within this figure, it is evident that the momentum algorithm exhibits excellent performance, particularly in terms of reducing the peak frequencies. For the front and right microphone, the performance of the peak reduction across the frequency spectrum is notably similar.

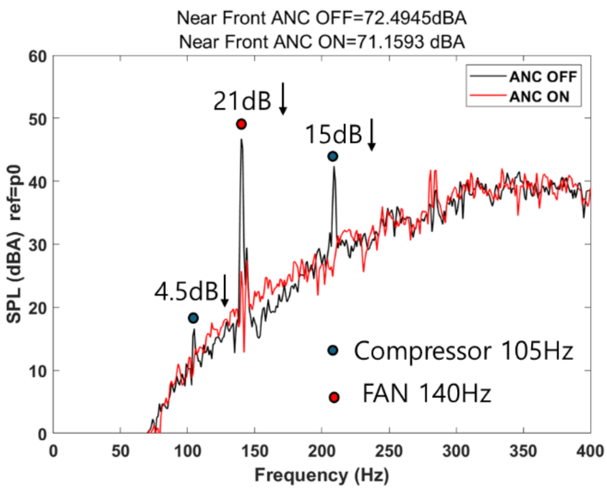

(a) Fourier transform of the front error microphone.

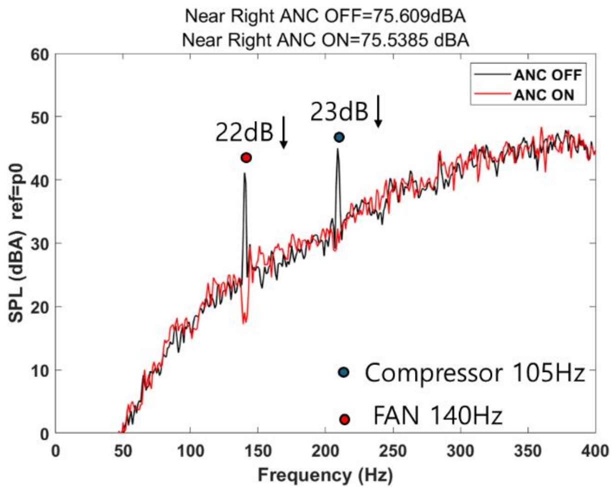

(b) Fourier transform of the right error microphone.

Figure 9. Fourier transform of the error microphones data without and with ANC.

The attenuation level of fan noise is up to 22dB at 140Hz and that of compressornoise is up to 23dB .

Attenuation levels of noise measured by front and right microphone are depicted as shown in Fig.10. Consequently Uncontrolled noise measured at far field microphones was also attended through ANC of near field noise.

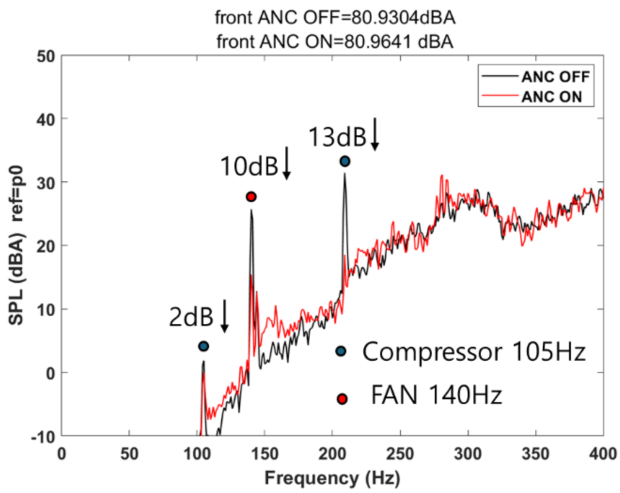

(a) Fourier transform of the front error microphone.

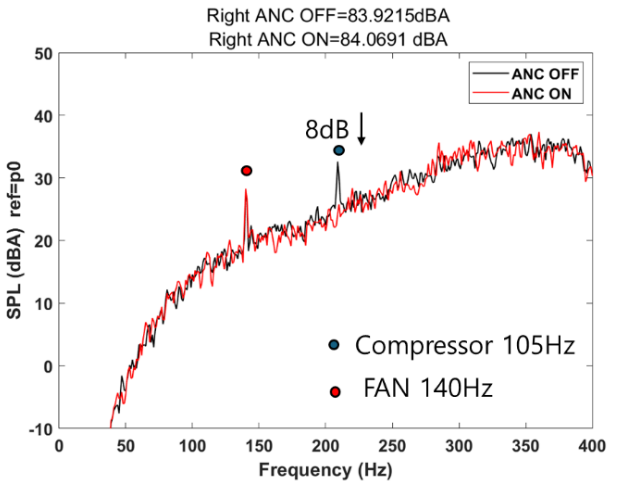

(b) Fourier transform of the right error microphone.

Figure 10. Fourier transform of the far field microphones data without and with ANC.

5. CONCLUSIONS

In this study, we present the implementation of a momentum algorithm within the HVAC system of an autonomous bus seat. The HVAC system is a significant source of vibroacoustic noise, predominantly within the 100 to 400 Hz frequency range. This noise is primarily due to the vibration of the compressor's shell at the rotation frequency and its harmonics, resulting in prominent peaks in the frequency response. To control these disruptive noises, an ANC system has been developed. The reference signal for the ANC system was derived from an accelerometer stuck to the compressor's shell. Noise level of HVAC system is attenuated up to 20dB at near filed and 10dB at far field respectively. The study concludes that the momentum algorithm is excellent in reducing the overall noise levels of the HVAC system.

6. ACKNOWLEDGMENTS

This work was supported by the grant funded by the Korea evaluation institute of industrial technology (KEIT) (No. 20018706).

7. REFERENCES

[1] Sen M Kuo and Dennis R Morgan. Active noise control systems, volume 4. Wiley, New York, 1996.

[2] DG Smith, MF Arnold, EW Ziegler, Kh Eghtesadi, and M Brown. A systems approach to appliance compressor quieting using active noise control techniques. 1992.

[3] Hwang, W., Oh, I., Kim, B., Park, S., & Ryu, K. (2006). A study on noise radiation from compressor shell.

[4] Widrow Bernard and D Stearns Samuel. Adaptive signal processing. Englewood Cliffs, NJ: Prentice Hall, 1985.

[5] JM Ku, WB Jeong, and C Hong. Active control of compressor noise in the machinery room of refrigerators. Noise Control Engineering Journal, 67(5):350–362, 2019.

[6] Ku, J. M., Jeong, W. B., & Hong, C. (2020). Controller design for active noise control of compressor by using the time window POCS technique. Journal of Mechanical Science and Technology, 34, 2693-2700.

[7] Meena, Shiv Ram, and C. S. Rai. "Effect of eigenvalue spread in noise cancellation of two sensory systems using adaptive algorithms." Journal of Statistics and Management Systems 23.1 (2020): 157-169.

[8] Burgess, John C. "Active adaptive sound control in a duct: A computer simulation." The Journal of the Acoustical Society of America 70.3 (1981): 715-726.

[9] Goran Nakerst, John Brennan, and Masudul Haque, "Gradient descent with momentum — to accelerate or to super-accelerate?", arXiv:2001.06472v1, (2020): 1-23.

[10] International Organization for Standardization. (2004). Acoustics — Noise test code for compressors and vacuum pumps — Engineering method (Grade 2) (ISO Standard No. 2151:2004). https://www.iso.org/standard/31316.html

[11] Shin, Kihong, and Joseph Hammond. Fundamentals of signal processing for sound and vibration engineers. John Wiley & Sons, 2008.

[12] Lee, S. K., Lee, S., Back, J., Shin, S. (2018). A New Method for Active Cancellation of Engine Order Noise in a Passenger Car. Appl. Sci. 8, 1394.

[13] H. W. Kim, H. S. Park, S. K. Lee and K. H. Shin, Modified-Filtered-u LMS Algorithm for Active Noise Control and Its Application to a Short Acoustic Duct, Mechanical Systems and Signal Processing 25 (2011) 475-484.